JOURNAL OF MULTIFUNCTIONAL MATERIALS & PHOTOSCIENCE
9(1), June 2018, pp. 39-48

White Emissions of $Ho^{3+}/Yb^{3+}/Tm^{3+}$ Tri-Doped $NaGd(MoO_4)_2$ Phosphors and Their Upconversion Photoluminescence Propreties

Won-Chun Oh, Ji Soon Park, Eung Gyun Kim, Chang Sung Lim*

Department of Advanced Materials Science & Engineering, Hanseo University, Seosan 356-706, Korea

Abstract: Microwave sol-gel based white phosphors of $NaGd_{1-x}(MoO_4)_2$ doped with appropriate additions of Yb^{3+} for a sensitizer and Ho^{3+}/Tm^{3+} for activators were successfully fabricated, and their spectroscopic characteristics were investigated. The resultant particles showed well-crystallized and homogeneous morphologies with 2-4 ìm of particle sizes. Under excitation derived from 980 nm, the final particles led to the formation of white emissions composed of the red, green, and blue emission features, which are resulted from the transitions of Tm^{3+} from the $^1G_4 \rightarrow {}^3H_6$ in the blue emission area, the transitions of Ho^{3+} from the $^5S_2/{}^5F_4 \rightarrow {}^5I_8$ in the green emission area, as well as the transitions of Ho^{3+} from the $^5F_5 \rightarrow {}^5I_8$ and the transitions of Tm^{3+} from the $^1G_4 \rightarrow {}^3F_4$ and $^3H_4 \rightarrow {}^3H_6$ in the red emission area. The dependence for pump power, chromaticity coordinates of CIE, and Raman spectroscopic feature of the synthesized phosphors were discussed.

Key words: White emission, $Ho^{3+}/Yb^{3+}/Tm^{3+}$ tri-doped, $NaGd(MoO_4)_2$ phosphors, Upconverion properties

Introduction

Recently, oxide-based phosphors derived from upconversion (UC) process are providing highly evaluated potentials due to unique luminescent characteristics and crystal structural stabilities in the important optoelectronic fields such as final products for laser generators, display compositions, LED, solar cell devices, and biological imaginations using luminescent materials [1-3]. In particular, Ln(Ln = Y^{3+}, Gd^{3+} and La^{3+})-doped binary $NaLn(MoO_4)_2$ compounds belong to the space group $I4_1/a$ with the tetragonal phase, and have the family of sheelite-type structure [4, 5]. The trivalent lanthanide ions are partially substituted into the crystalline lattices of the tetragonal double tungstate crystal phase. The possible doping could be attributed to the very similar radii of the trivalent lanthanide ions and bring excellent properties for UC photoluminescence [6]. Multicolor and white light emissions can be generated via a tri-doping system based on the blue, green, and red emission bands. Many lanthanide doping materials, such as laser active Ho^{3+} and Tm^{3+},

* Corresponding author: *cslim@hanseo.ac.kr*

are employed as an activator in luminescent centers for Yb^{3+} as a sentitizer, because of their unique electronic energy levels. The tri-doped Yb^{3+}, Ho^{3+}, and Tm^{3+} ions can remarkably enhance the UC efficiency for the shift from infrared to visible light because of the efficiency of the energy transfer from Yb^{3+} to Ho^{3+} and Yb^{3+} to Tm^{3+}. Ho^{3+} exhibits $^5S_2/\ ^5F_4 \rightarrow\ ^5I_8$ transitions in the green region, $^5F_5 \rightarrow\ ^5I_8$ transitions in the red region in the upconversion process, and Tm^{3+} shows the $^1G_4 \rightarrow\ ^3H_6$ transitions in the blue region, and $^1G_4 \rightarrow\ ^3F_4$ and $^3H_4 \rightarrow\ ^3H_6$ transitions in the red region [7-9]. These ions are effectively doped into the crystal lattices of the tetragonal phase because of the similar radii of the trivalent rare-earth ions; this results in high red-emitting efficiency, and superior thermal and chemical stability in the white emitting diode.

For preparation of the binary molybdate $NaLn(MoO_4)_2$, several specific processes have been developed, including solid-state reactions [10-13], the sol-gel method [14, 15], the Czochralski method [16-19], the hydrothermal method [20-24], the microwave assisted hydrothermal method [25], and pulse laser deposition [26]. Compared to the usual methods, microwave synthesis has the advantages of a very short reaction time, small-size particles, narrow particle-size distribution, and high purity of the final polycrystalline samples [27]. However, the synthesis of $Ho^{3+}/Yb^{3+}/Tm^{3+}$ tri-doped $NaGd(MoO_4)_2$ phosphors via the microwave sol-gel route has not been reported. In this study, the double molybdate $NaGd(MoO_4)_2$ phosphors with the proper doping concentrations of Ho^{3+}, Yb^{3+} and Tm^{3+} ($x = Ho^{3+} + Yb^{3+} + Tm^{3+}$, $Ho^{3+} = 0.04, 0.03, 0.02, 0.01$, $Yb^{3+} = 0.35, 0.40, 0.45, 0.50$ and $Tm^{3+} = 0.01, 0.02, 0.03, 0.04$) were successfully prepared by the microwave sol-gel method, followed by heat treatment. The synthesized particles were characterized by X-ray diffraction (XRD) and scanning electron microscopy (SEM). The pump power dependence of the UC emission intensity and Commission Internationale de L'Eclairage (CIE) chromatic coordinates were evaluated in detail. The optical properties were examined comparatively using photoluminescence (PL) emission and Raman spectroscopy.

Experimental

Appropriate stoichiometric amounts of $Na_2MoO_4{\cdot}2H_2O$ (99%, Sigma-Aldrich, USA), $Gd(NO_3)_3{\cdot}6H_2O$ (99%, Sigma-Aldrich, USA), $(NH_4)_6Mo_7O_{24}{\cdot}4H_2O$ (99%, Alfa Aesar, USA), $Ho(NO_3)_3{\cdot}5H_2O$ (99.9%, Sigma-Aldrich, USA), $Yb(NO_3)_3{\cdot}5H_2O$ (99.9%, Sigma-Aldrich, USA), $Tm(NO_3)_3{\cdot}\ 5H_2O$ (99.9%, Sigma-Aldrich, USA), citric acid (99.5%, Daejung Chemicals, Korea), NH_4OH (A.R.), ethylene glycol (A.R.), and distilled water were used to prepare the compounds. To prepare $NaGd_{0.60}(MoO_4)_2{:}Ho_{0.04}/Yb_{0.35}/Tm_{0.01,}$ 0.2 mol% $Na_2MoO_4{\cdot}2H_2O$ and 0.114 mol% $(NH_4)_6Mo_7O_{24}{\cdot}4H_2O$ were dissolved in 20 mL of ethylene glycol and 80 mL of 5M NH_4OH under vigorous stirring and heating. Subsequently, 0.24 mol% $Gd(NO_3)_3{\cdot}6H_2O$ with 0.016 mol% $Ho(NO_3)_3{\cdot}5H_2O$, 0.14 mol% $Yb(NO_3)_3{\cdot}5H_2O$, 0.004 mol% $Tm(NO_3)_3{\cdot}5H_2O$, and citric acid (with a molar ratio of citric acid to total metal ions of 2:1) were dissolved in 100 mL of distilled water under vigorous stirring and heating. Then, the solutions were mixed together under vigorous stirring and heating at 80 to 100°C. Finally, highly transparent solutions were obtained and adjusted to *p*H = 7-8 by the addition of 8M NH_4OH. In order to prepare $NaGd_{0.55}(MoO_4)_2{:}Ho_{0.03}/Yb_{0.40}/Tm_{0.02,}$ the mixture of 0.22 mol% $Gd(NO_3)_3{\cdot}6H_2O$ with

0.012 mol% $Ho(NO_3)_3{\cdot}5H_2O$, 0.16 mol% $Yb(NO_3)_3{\cdot}5H_2O$, and 0.008 mol% $Tm(NO_3)_3{\cdot}5H_2O$ was used to create the rare-earth solution. In order to prepare $NaGd_{0.50}(MoO_4)_2{:}Ho_{0.02}/Yb_{0.45}/Tm_{0.03,}$ the mixture of 0.20 mol% $Gd(NO_3)_3{\cdot}6H_2O$ with 0.008 mol% $Ho(NO_3)_3{\cdot}5H_2O$, 0.18 mol% $Yb(NO_3)_3{\cdot}5H_2O$, and 0.012 mol% $Tm(NO_3)_3{\cdot}5H_2O$ was used to create the rare-earth solution. In order to prepare $NaGd_{0.45}(MoO_4)_2{:}Ho_{0.01}/Yb_{0.50}/Tm_{0.04,}$ the rare-earth containing solution was generated using 0.18 mol% $Gd(NO_3)_3{\cdot}6H_2O$ with 0.004 mol% $Ho(NO_3)_3{\cdot}5H_2O$, 0.20 mol% $Yb(NO_3)_3{\cdot}5H_2O$, and 0.016 mol% $Tm(NO_3)_3{\cdot}5H_2O$.

The transparent solutions were placed in a microwave oven operating at a frequency of 2.45 GHz with a maximum output power of 1250 W for 30 min. The working cycle of the microwave reaction was controlled very precisely using a regime of 40 s on and 20 s off for 15 min, followed by further treatment of 30 s on and 30 s off for 15 min. The samples were treated with ultrasonic radiation for 10 min to produce a light-yellow transparent sol. After this, the light-yellow transparent sols were dried at 120°C in a dry oven to obtain black dried gels, which were ground and heat-treated at 800°C for 16 h with 100°C intervals between 600 and 800°C. Finally, pink particles were obtained for the doped compositions. The phase composition of the synthesized particles was identified using XRD (D/MAX 2200, Rigaku, Japan). The microstructure and surface morphology of the synthesized particles were observed using SEM (JSM-5600, JEOL, Japan). The PL spectra were recorded using a spectrophotometer (Perkin Elmer LS55, UK) at room temperature. Raman spectroscopy measurements were performed using a LabRam Aramis (Horiba Jobin-Yvon, France). The 514.5-nm line of an Ar ion laser was used as the excitation source, and the power on the samples was kept at 0.5 mW.

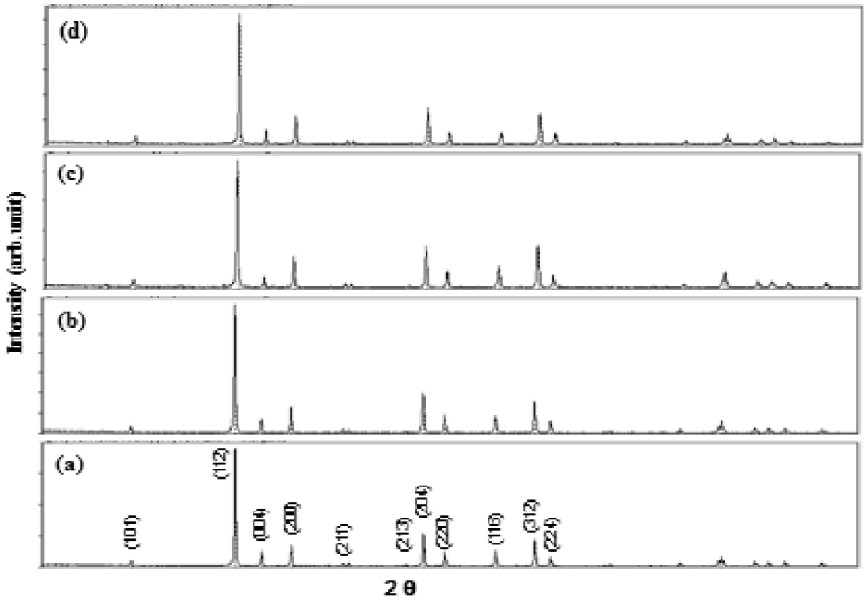

Figure 1: X-ray diffraction patterns of the (a) $NaGd_{0.60}(MoO_4)_2{:}Ho_{0.04}/Yb_{0.35}/Tm_{0.01,}$ (b) $NaGd_{0.55}(MoO_4)_2{:}Ho_{0.03}/Yb_{0.40}/Tm_{0.02,}$ (c) $NaGd_{0.50}(MoO_4)_2{:}Ho_{0.02}/Yb_{0.45}/Tm_{0.03,}$ and (d) $NaGd_{0.45}(MoO_4)_2{:}Ho_{0.01}/Yb_{0.50}/Tm_{0.04,}$ particles

Results and Discussion

Fig. 1 shows the X-ray diffraction patterns of the synthesized (a) $NaGd_{0.60}(MoO_4)_2$:$Ho_{0.04}$/$Yb_{0.35}$/$Tm_{0.01,}$ (b) $NaGd_{0.55}(MoO_4)_2$:$Ho_{0.03}$/$Yb_{0.40}$/$Tm_{0.02,}$ (c) $NaGd_{0.50}(MoO_4)_2$:$Ho_{0.02}$/$Yb_{0.45}$/$Tm_{0.03}$, and (d) $NaGd_{0.45}(MoO_4)_2$:$Ho_{0.01}$/$Yb_{0.50}$/$Tm_{0.04}$ particles. All the XRD peaks could be assigned to the tetragonal-phase $NaGd(MoO_4)_2$ with the space group of $I4_1/a$, which was in good agreement with the crystallographic data of $NaGd(MoO_4)_2$ (JCPDS 25-0828). $NaGd(MoO_4)_2$ as a member of double molybdate family has a sheelite structure with the lattice constants of a=5.235 Å and c=11.538 Å [20]. In pure $NaGd(MoO_4)_2$ crystals, the unit cell decrease occurs because of the substitution of Ho^{3+} (R = 1.015 Å), Yb^{3+} (R = 0.985 Å) and Tm^{3+} (R = 0.994 Å) ions in the Gd^{3+} (R=1.053 Å) sites [28]. Post heat-treatment plays an important role in a well-defined crystallized morphology. To achieve a well-defined crystalline morphology of $NaGd_{0.60}(MoO_4)_2$:$Ho_{0.04}$/$Yb_{0.35}$/$Tm_{0.01,}$ $NaGd_{0.55}(MoO_4)_2$:$Ho_{0.03}$/$Yb_{0.40}$/$Tm_{0.02,}$ $NaGd_{0.50}(MoO_4)_2$:$Ho_{0.02}$/$Yb_{0.45}$/$Tm_{0.03}$, and $NaGd_{0.45}(MoO_4)_2$:$Ho_{0.01}$/$Yb_{0.50}$/$Tm_{0.04}$ particles, phases need to be heat treated at 800°C for 16 h. It is assumed that the doping amount of Ho^{3+}/Yb^{3+}/Tm^{3+} has a great effect on the crystalline cell volume of the $NaGd(MoO_4)_2$, because of the different ionic sizes. That is, the obtained samples possess a tetragonal phase after partial substitution of Gd^{3+} by Ho^{3+}, Yb^{3+}, and Tm^{3+} ions, which are effectively doped into the crystal lattices of the $NaGd(MoO_4)_2$ phase because of the similar radii of Gd^{3+}, Ho^{3+}, Yb^{3+}, and Tm^{3+}.

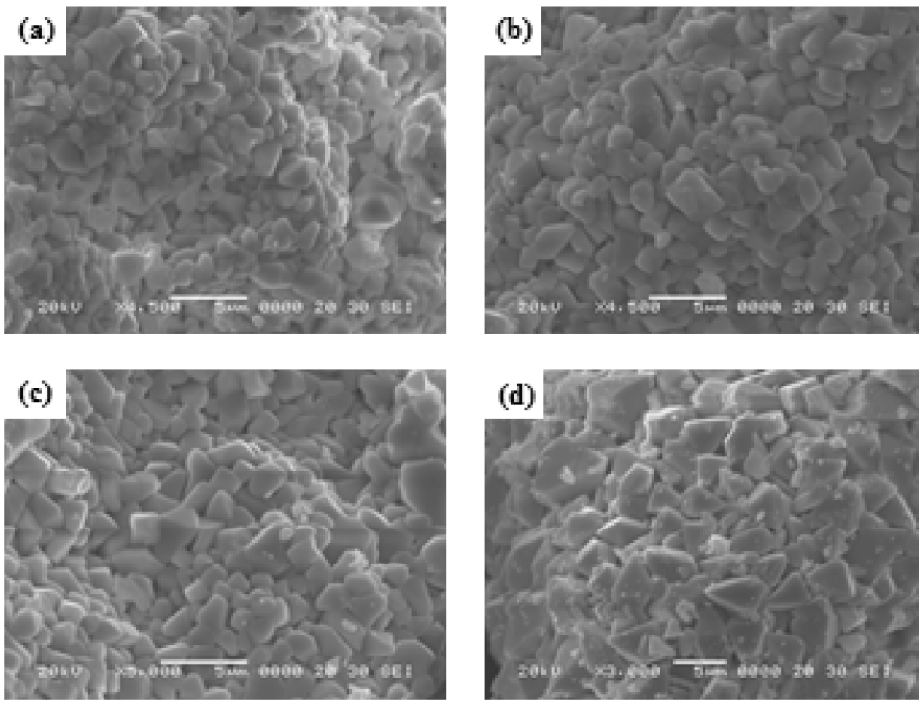

Figure 2: Scanning electron microscopy images of the synthesized (a) $NaGd_{0.60}(MoO_4)_2$:$Ho_{0.04}$/$Yb_{0.35}$/$Tm_{0.01,}$ (b) $NaGd_{0.55}(MoO_4)_2$:$Ho_{0.03}$/$Yb_{0.40}$/$Tm_{0.02,}$ (c) $NaGd_{0.50}(MoO_4)_2$:$Ho_{0.02}$/$Yb_{0.45}$/$Tm_{0.03}$, and (d) $NaGd_{0.45}(MoO_4)_2$:$Ho_{0.01}$/$Yb_{0.50}$/$Tm_{0.04,}$ particles

Fig. 2 shows SEM images of the synthesized (a) $NaGd_{0.60}(MoO_4)_2:Ho_{0.04}/Yb_{0.35}/Tm_{0.01,}$ (b) $NaGd_{0.55}(MoO_4)_2:Ho_{0.03}/Yb_{0.40}/Tm_{0.02,}$ (c) $NaGd_{0.50}(MoO_4)_2:Ho_{0.02}/Yb_{0.45}/Tm_{0.03}$, and (d) $NaGd_{0.45}(MoO_4)_2:Ho_{0.01}/Yb_{0.50}/Tm_{0.04}$ particles. The as-synthesized samples have similar morphologies and no discrepancy in morphological features, showing well crystallized and homogeneous microcrystalline morphology with a particle size of 2-4 ìm. In particular, the strongly agglomerated morphology of the particles can be observed by the atom inter-diffusion between the grains. The microwave sol-gel method in application to the double molybdates provides the energy to synthesize the bulk of the material uniformly, so that fine particles with controlled morphology can be fabricated in a short time. The method is a cost-effective way to fabricate highly homogeneous products with easy scale-up. It is a viable alternative for the rapid synthesis of UC particles. This suggests that the microwave sol-gel route is suitable for the creation of homogeneous $NaGd_{1-x}(MoO_4)_2:Ho^{3+}/Yb^{3+}/Tm^{3+}$ crystallites.

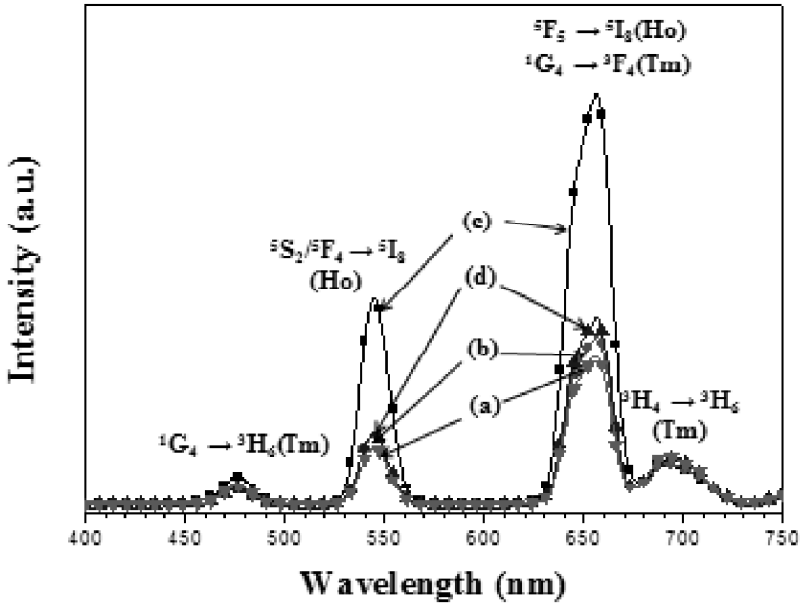

Figure 3: Upconversion photoluminescent emission spectra of (a) $NaGd_{0.60}(MoO_4)_2:Ho_{0.04}/Yb_{0.35}/Tm_{0.01,}$ (b) $NaGd_{0.55}(MoO_4)_2:Ho_{0.03}/Yb_{0.40}/Tm_{0.02,}$ (c) $NaGd_{0.50}(MoO_4)_2:Ho_{0.02}/Yb_{0.45}/Tm_{0.03}$, and (d) $NaGd_{0.45}(MoO_4)_2:Ho_{0.01}/Yb_{0.50}/Tm_{0.04}$ particles excited under 980 nm at room temperature

Fig. 3 shows the UC photoluminescence emission spectra of the as-prepared (a) $NaGd_{0.60}(MoO_4)_2:Ho_{0.04}/Yb_{0.35}/Tm_{0.01,}$ (b) $NaGd_{0.55}(MoO_4)_2:Ho_{0.03}/Yb_{0.40}/Tm_{0.02,}$ (c) $NaGd_{0.50}(MoO_4)_2:Ho_{0.02}/Yb_{0.45}/Tm_{0.03}$, and (d) $NaGd_{0.45}(MoO_4)_2:Ho_{0.01}/Yb_{0.50}/Tm_{0.04}$ particles. Under excitation at 980 nm at room temperature, the doped particles exhibited white emissions based on blue, green, and red emission bands, which correspond to the $^1G_4 \rightarrow {}^3H_6$ transitions of Tm^{3+} in the blue region, the $^5S_2/{}^5F_4 \rightarrow {}^5I_8$ transitions of Ho^{3+} in the green region, and the $^5F_5 \rightarrow {}^5I_8$ transitions of Ho^{3+}, as well as the $^1G_4 \rightarrow {}^3F_4$ and $^3H_4 \rightarrow {}^3H_6$ transitions of Tm^{3+}, in the red region. The UC intensity of (c) $NaGd_{0.50}(MoO_4)_2:Ho_{0.02}/Yb_{0.45}/Tm_{0.03}$

provides the strongest 545-nm emission band in the green region, and the strongest 655-nm emission band in the red region because of the appropriate ratio of Yb^{3+}: Ho^{3+}+Tm^{3+} = 9:1. Thus, the optimal Yb^{3+}: Ho^{3+}+Tm^{3+} ratio is as high as 9:1 for the white emitting diode based on the blue, green, and red emissions.

The logarithmic scale dependence of the UC emission intensities at 475, 545, 655, and 695 nm on the working pump power over the range of 20 to 110 mW in the $NaGd_{0.50}(MoO_4)_2$:$Yb_{0.02}$/$Ho_{0.45}$/$Tm_{0.03}$ sample is shown in Fig. 4. In the UC process, the UC emission intensity is proportional to the slope value n of the irradiation pumping power, where n is the number of pumped photons required to produce UC emission [29]:

$$I \propto P^n \tag{1}$$

$$\mathrm{Ln}I \propto n\mathrm{Ln}P \tag{2}$$

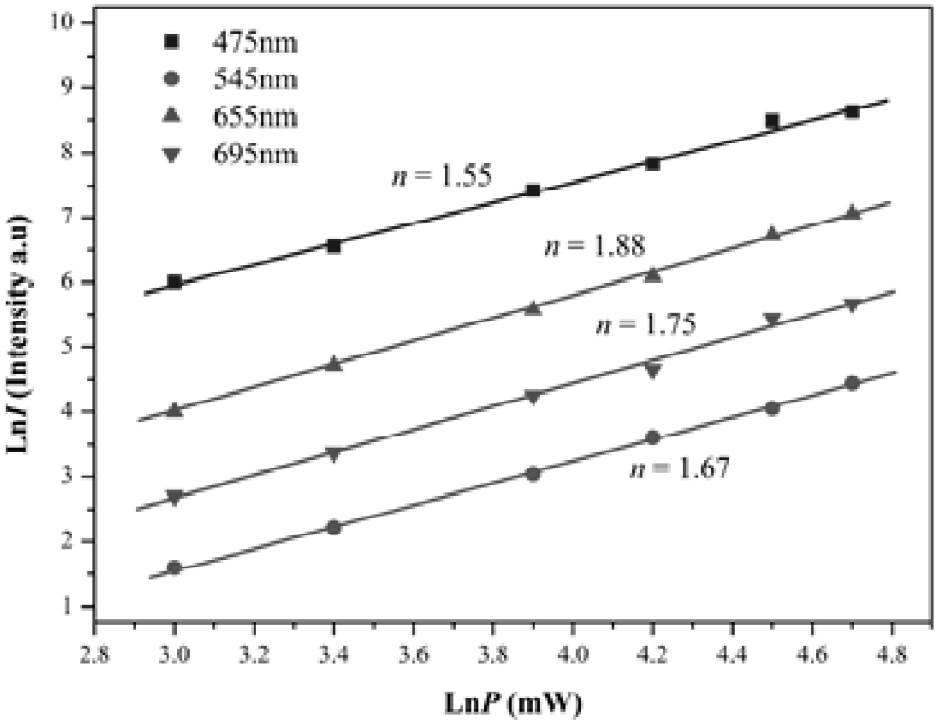

Figure 4: Logarithmic scale dependence of the upconversion emission intensity on the pump power in the range from 20 to 110 mW at 475, 545, 655, and 695 nm in the $NaGd_{0.50}(MoO_4)_2$:$Ho_{0.02}$/$Yb_{0.45}$/$Tm_{0.03}$ sample

where I is the UC luminescent intensity, and P is the laser pumping power. As is evident from Fig. 4, the slope value calculations indicate n = 1.55 for green emission at 475 nm, n = 1.67 for green emission at 545 nm, and n = 1.88 and 1.75 for red emissions at 655 and 695 nm, respectively.

(A)

(a)	
x	y
0.347	0.354
(b)	
x	y
0.339	0.341
(c)	
x	y
0.340	0.341
(d)	
x	y
0.339	0.339

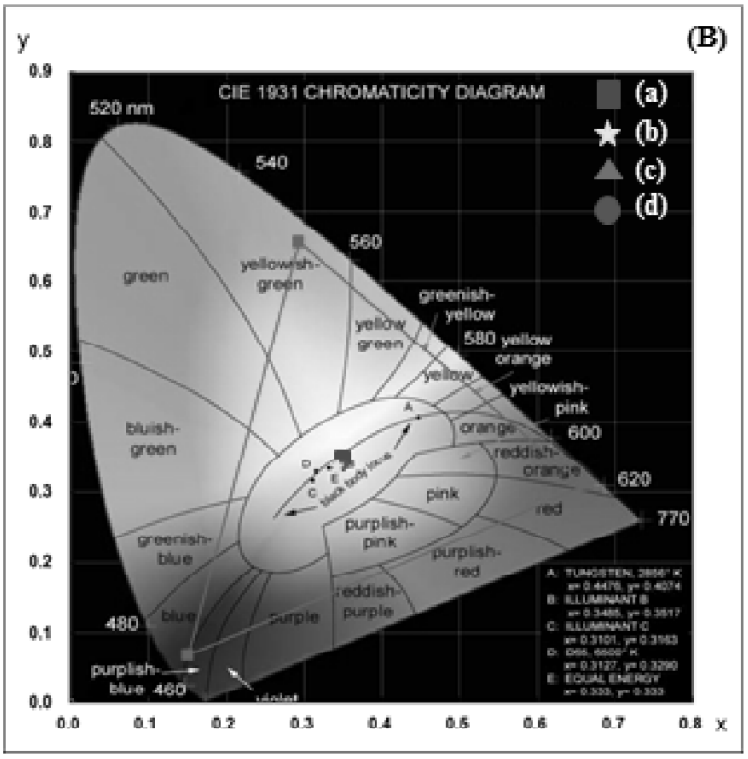

Figure 5: (A) Calculated chromaticity coordinates (*x, y*) values and (B) CIE chromaticity diagram for $NaGd_{1-x}(MoO_4)_2:Ho^{3+}/Yb^{3+}/Tm^{3+}$ phosphors. The inset shows the emission points for the sample synthesized (a) $NaGd_{0.60}(MoO_4)_2:Ho_{0.04}/Yb_{0.35}/Tm_{0.01,}$ (b) $NaGd_{0.55}(MoO_4)_2:Ho_{0.03}/Yb_{0.40}/Tm_{0.02,}$ (c) $NaGd_{0.50}(MoO_4)_2:Ho_{0.02}/Yb_{0.45}/Tm_{0.03}$, and (d) $NaGd_{0.45}(MoO_4)_2:Ho_{0.01}/Yb_{0.50}/Tm_{0.04,}$ particles

Fig. 5 shows (A) calculated chromaticity coordinates (*x, y*) values and (B) CIE chromaticity diagram for (a) $NaGd_{0.60}(MoO_4)_2:Ho_{0.04}/Yb_{0.35}/Tm_{0.01,}$ (b) $NaGd_{0.55}(MoO_4)_2:Ho_{0.03}/Yb_{0.40}/Tm_{0.02,}$ (c) $NaGd_{0.50}(MoO_4)_2:Ho_{0.02}/Yb_{0.45}/Tm_{0.03}$, and (d) $NaGd_{0.45}(MoO_4)_2:Ho_{0.01}/Yb_{0.50}/Tm_{0.04}$ particles. In Fig. 6 (A) the calculated chromaticity coordinates (*x, y*) and (B) CIE chromaticity diagrams are shown for the compositions (a) $NaGd_{0.60}(MoO_4)_2:Ho_{0.04}/Yb_{0.35}/Tm_{0.01,}$ (b) $NaGd_{0.55}(MoO_4)_2:Ho_{0.03}/Yb_{0.40}/Tm_{0.02,}$ (c) $NaGd_{0.50}(MoO_4)_2:Ho_{0.02}/Yb_{0.45}/Tm_{0.03}$, and (d) $NaGd_{0.45}(MoO_4)_2:Ho_{0.01}/Yb_{0.50}/Tm_{0.04}$. The triangle in Fig. 6(B) indicates standard coordinates for blue, green, and red. The inset in Fig. 6(B) shows the chromaticity points for the samples (a), (b), (c), and (d). The chromaticity coordinates (*x, y*) are strongly dependent on the $Ho^{3+}/Yb^{3+}/Tm^{3+}$ concentration ratio. As shown in Fig. 6(A), the calculated chromaticity coordinates $x = 0.347$ and $y = 0.355$ for (a) $NaGd_{0.60}(MoO_4)_2:Ho_{0.04}/Yb_{0.35}/Tm_{0.01,}$ $x = 0.339$ and $y = 0.342$ for (b) $NaGd_{0.55}(MoO_4)_2:Ho_{0.03}/Yb_{0.40}/Tm_{0.02,}$ $x = 0.340$ and $y = 0.341$ for (c) $NaGd_{0.50}(MoO_4)_2:Ho_{0.02}/Yb_{0.45}/Tm_{0.03}$, and $x = 0.339$ and $y = 0.339$ for (d) $NaGd_{0.45}(MoO_4)_2:Ho_{0.01}/Yb_{0.50}/Tm_{0.04}$, corresponding to the standard equal-energy point in the CIE diagram in Fig. 6(B).

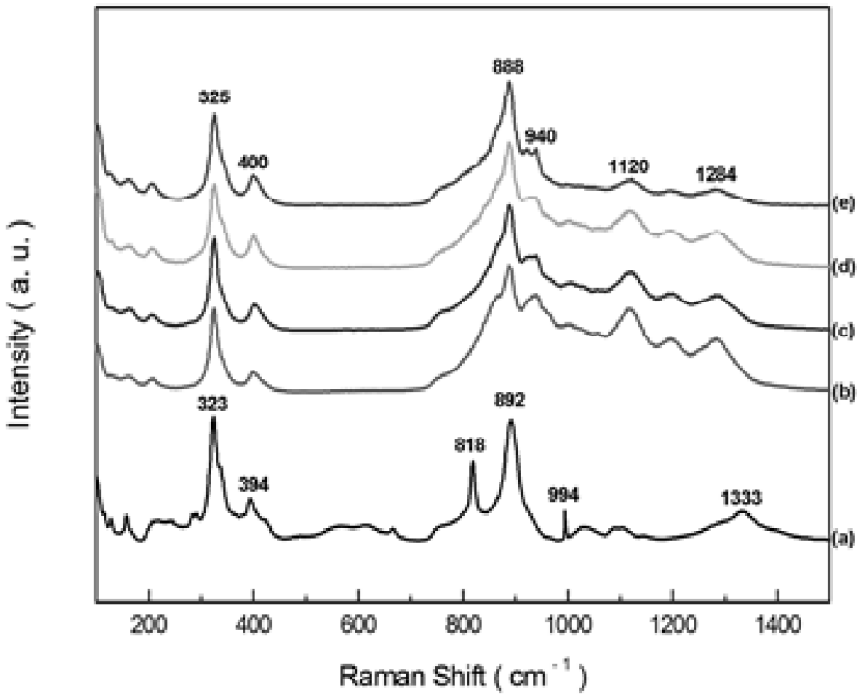

Figure 6: Raman spectra of the synthesized (a) pure $NaGd(MoO_4)_2$, (b) $NaGd_{0.60}(MoO_4)_2:Ho_{0.04}/Yb_{0.35}/Tm_{0.01}$, (c) $NaGd_{0.55}(MoO_4)_2:Ho_{0.03}/Yb_{0.40}/Tm_{0.02}$, (d) $NaGd_{0.50}(MoO_4)_2:Ho_{0.02}/Yb_{0.45}/Tm_{0.03}$, and (e) $NaGd_{0.45}(MoO_4)_2:Ho_{0.01}/Yb_{0.50}/Tm_{0.04}$ particles excited by the 514.5-nm line of an Ar ion laser at 0.5 mW

Fig. 6 shows the Raman spectra of the synthesized (a) pure $NaGd(MoO_4)_2$, (b) $NaGd_{0.60}(MoO_4)_2:Ho_{0.04}/Yb_{0.35}/Tm_{0.01}$, (c) $NaGd_{0.55}(MoO_4)_2:Ho_{0.03}/Yb_{0.40}/Tm_{0.02}$, (d) $NaGd_{0.50}(MoO_4)_2:Ho_{0.02}/Yb_{0.45}/Tm_{0.03}$, and (e) $NaGd_{0.45}(MoO_4)_2:Ho_{0.01}/Yb_{0.50}/Tm_{0.04}$ particles excited by the 514.5-nm line of an Ar ion laser at 0.5 mW. The internal modes for the (a) pure $NaGd(MoO_4)_2$ particles were detected at 323, 394, 818, 892, 994, and 1333 cm^{-1}. The well-resolved sharp peaks for the $NaGd(MoO_4)_2$ indicate a high crystallinity state of the synthesized particles. The internal vibration-mode frequencies depend on the lattice parameters and the strength of the partially covalent bond between the cation and molecular ionic group MO_4. The Raman spectrum of the $NaGd(MoO_4)_2$ crystal in Fig. 6(a) shows the typical molybdate compounds, which are divided into two parts with a wide empty gap of 400~800 cm^{-1} [30-33]. The stretching vibrations of Mo-O bonds are observed at 818~994 cm^{-1}. For these stretching vibrations, strong mixing occurs between the Mo-O bonds and the MoO_4. The bands at 323 and 394 cm^{-1} could be assumed to originate from vibrations of the longer Mo-O bonds, which are employed in the formation of the Mo-Mo bridge. The translational vibration motion of the Na^{3+} ions is observed around 200~300 cm^{-1}, whereas the Gd^{3+} translations were located below 180 cm^{-1} [32, 33]. The Raman spectra of the doped particles indicate the very strong and dominant peaks at higher frequencies of 888, 940, 1120, and 1284 cm^{-1} and at lower frequencies of 325 and 400 cm^{-1}. These strong

disordered peaks at higher and lower frequencies are attributed to the superimpositions and the concentration-quenching effect of the Ho^{3+} and Tm^{3+} ions [34, 35]. These results lead to high emitting efficiency and superior thermal and chemical stability, and these materials can be considered potentially active components in white LED applications.

Conclusions

Microwave sol-gel derived white phosphors of $NaGd_{1-x}(MoO_4)_2$ doped with Yb^{3+} for a sensitizer and Ho^{3+}/Tm^{3+} for activators were successfully fabricated. The resultant particles after annealing at 800°C for 16 h provided well-crystallized and fine morphologies with 2-4 ìm of particle sizes. Under excitation derived from 980 nm, the final particles led to the formation of white emissions composed of the red, green, and blue emission features, which are resulted from the transitions of Tm^{3+} from the $^1G_4 \rightarrow {}^3H_6$ in the blue emission area, the transitions of Ho^{3+} from the $^5S_2/{}^5F_4 \rightarrow {}^5I_8$ in the green emission area, as well as the transitions of Ho^{3+} from the $^5F_5 \rightarrow {}^5I_8$ and the transitions of Tm^{3+} from the $^1G_4 \rightarrow {}^3F_4$ and $^3H_4 \rightarrow {}^3H_6$ in the red emission area. The calculations of the slope value indicated n = 1.55 for green emission at 475 nm, n = 1.67 for green emission at 545 nm, and n = 1.88 and 1.75 for red emissions at 655 and 695 nm, respectively. These strong disordered Raman spectroscopic frequencies were attributed to the superimpositions and the effect of concentration-quenching for the activators for Ho^{3+} and Tm^{3+} ions.

Acknowledgment

This research was supported by the Basic Science Research Program through the National Research Foundation of Korea (NRF) funded by the Ministry of Education (2015-R1D1A1A01058813)

References

[1] C. S. Lim, A. Aleksandrovsky, M. Molokeev, A. Oreshonkov, V. Atuchin, Phys. Chem. Chem. Phys., 17, 19278 (2015).

[2] M. Wang, G. Abbineni, A. Clevenger, C. Mao, S. Xu, Nanomedicine: Nanotech. Biology, and Medicine, **7,** 710 (2011).

[3] C. S. Lim, A. Aleksandrovsky, M. Molokeev, A. Oreshonkov, D. Ikonnikov, V. Atuchin, Dalton Transactions, 45, 15541 (2016).

[4] L. Li, W. Zi, H. Yu, S. Gan, G. Ji, H. Zou, X. Xu, J. Lumin., 143, 14 (2013).

[5] C. Ming, F. Song, L. Yan, Opt. Comm., 286, 217 (2013).

[6] C.S. Lim, A. Aleksandrovsky, M. Molokeev, A. Oreshonkov, V. Atuchin, J. Solid State Chemistry, 228, 160 (2015).

[7] J. Jin, K. Yang, J. Su, Z. Si, J. Lumin., 159, 178 (2015).

[8] Y. Xu, Y. Wang, L. Xing, X. Tan, Optics & Laser Tech., 54, 50 (2013).

[9] D. Li, Y. Wang, X. Zhang, G.Shi, G. Liu, Y. Song, J. Alloys Compd., 550, 509 (2013).

[10] J. Tang, C. Cheng, Y. Chen, Y. Huang, J. Alloys Compd,. 609, 68 (2014).

[11] W. Zhang, J. Li, Y. Wang, J. Long, K. Qiu, J. Alloys Compd., 635, 16 (2015).

[12] F. Mo, L. Zhou, Q. Pang, F. Gong, Z. Liang, Ceram. Inter., 38, 6289 (2012).

[13] G. Li, S. Lan, L. Li, M. Li, W. Bao, H. Zou, X. Xu, S. Gan, J. Alloys Compd., 513, 145 (2012).

[14] J. Liao, H. Huang, H. You, X. Qiu, Y. Li, B. Qui, H-R Wen, Mater. Res. Bull., 45, 1145 (2010).

[15] F. Cao, L. Li, Y. Tian, X. Wu, Optics Laser Tech., 55, 6 (2014).

[16] G.M. Kuz'micheva, D.A. Lis, K.A. Subbotin, V.B. Rybakov, E.V. Zharikov, J. Crys. Growth, 275, e1835 (2005).

[17] X. Lu, Z. You, J. Li, Z. Zhu, G. Jia, B. Wu, C. Tu, J. Alloys Compd., 458, 462 (2008).

[18] X. Li, Z. Lin, L. Zhang, G. Wang, J. Crys. Growth, 290, 670 (2006).

[19] Y. K.Voron'ko, K.A. Subbotin, V.E. Shukshin, D.A. Lis, S.N. Ushakov, A.V. Popov, E.V. Zharikov, Opt. Mater., 29, 246 (2009).

[20] H. Lin, X. Yan, X. Wang, J. Sol. State. Chem., 204, 266 (2013).

[21] G. Li, L. Li, M. Li, W. Bao, Y. Song, S. Gan, H. Zou, X. Xu, J. Alloys Compd., 550, 1 (2013).

[22] Y. Huang, L. Zhou, L. Yang, Z. Tang, Opt. Mater., 33, 777 (2011).

[23] L. Li, W. Zi, G. Li, S. Lan, G. Ji, S. Gan, H. Zou, X. Xu, J. Sol. State Chem., 191, 175 (2012).

[24] Y. Tian, B. Chen, B. Tian, J. Sun, X. Li, J. Zhang, L. Cheng, H. Zhong, Q. Meng, R. Hua, Physica B., 407, 2556 (2012).

[25] J. Zhang, X. Wang, X. Zhang, X. Zhao, X. Liu, L. Peng, Inorg. Chem. Commun., 14, 1723 (2011).

[26] S.W. Park, B.K. Moon, B.C. Choi, J.H. Jeong, J.S. Bae, K.H. Kim, Curr. Appl. Phys., 12, S150 (2012).

[27] C.S. Lim, Mater. Res. Bull., 47, 4225 (2012).

[28] R. D. Shannon, Acta Cryst., A32, 751 (1976).

[29] H. Guo, N. Dong, M. Yin, W. Zhang, L. Lou, S. Xia, J. Phys. Chem. B, 108, 19205 (2004).

[30] V.V. Atuchin, V.G. Grossman, S.V. Adichtchev, N.V. Surovtsev, T.A. Gavrilova, B.G. Bazarov, Opt. Mater., 34, 812 (2012).

[31] A.A. Savina, V.V. Atuchin, S.F. Solodovnikov, Z.A. Solodovnikova, A.S. Krylov, E.A. Maximovskiy, M.S. Molokeev, A.S. Oreshonkov, A.M. Pugachev, E.G. Khaikina, J. Solid State Chem., 225, 53 (2015).

[32] V.V. Atuchin, O.D. Chimitova, T.A. Gavrilova, M.S. Molokeev, Sung-Jin Kim, N.V. Surovtsev, B.G. Bazarov, J. Crys. Growth, 318, 683 (2011).

[33] V.V. Atuchin, O.D. Chimitova, S.V. Adichtchev, J.G. bazarov, T.A. Gavrilova, M.S. Molokeev, N.V. Surovtsev, Zh.G. Bazarova, Mater. Lett., 106, 26 (2013).

[34] C. S. Lim, A, Aleksandrovsky, M. Molokeev, A. Oreshonkov, V. Atuchin, J. Alloys Compds., 695, 737 (2017).

[35] C. S. Lim, A, Aleksandrovsky, M. Molokeev, A. Oreshonkov, V. Atuchin, Mater. Lett., 181, 38 (2016).